Multiresonant metasurfaces for arbitrarily broad bandwidth pulse chirping and dispersion compensation

Odysseas Tsilipakos and Thomas Koschny

Phys. Rev. B **107**, 165408 — Published 10 April 2023

DOI: 10.1103/PhysRevB.107.165408

Multiresonant metasurfaces for arbitrary broad bandwidth pulse chirping and dispersion compensation

Odysseas Tsilipakos[1, 2, *] and Thomas Koschny[3]

[1] *Theoretical and Physical Chemistry Institute, National Hellenic Research Foundation, GR-11635 Athens, Greece*
[2] *Institute of Electronic Structure and Laser, Foundation for Research and Technology Hellas, GR-70013 Heraklion, Greece*
[3] *Ames Laboratory—U.S. DOE and Department of Physics and Astronomy, Iowa State University, Ames, Iowa 50011, USA*

(Dated: March 31, 2023)

We show that ultrathin metasurfaces with a specific multiresonant response can enable simultaneously arbitrarily-strong and arbitrarily-broadband dispersion compensation, pulse (de-)chirping and compression or broadening. This breakthrough overcomes the fundamental limitations of both conventional non-resonant approaches (bulky) and modern singly-resonant metasurfaces (narrowband) for quadratic phase manipulations of electromagnetic signals. The required non-uniform trains of resonances in the electric and magnetic sheet conductivities that completely control phase delay, group delay, and chirp, are rigorously derived and the limitations imposed by fundamental physical constraints are thoroughly discussed. Subsequently, a practical, truncated approximation by finite sequences of physically-realizable linear resonances is constructed and the associated error is quantified. By appropriate spectral ordering of the resonances, operation can be achieved either in transmission or reflection mode, enabling full space coverage. The proposed concept is not limited to dispersion compensation, but introduces a generic and powerful ultrathin platform for the spatio-temporal control of broadband real-world signals with a myriad of applications in modern optics, microwave photonics, radar and communication systems.

I. INTRODUCTION

Metasurfaces (MSs), ultrathin artificial media composed of subwavelength resonant meta-atoms, are being extensively studied for a myriad of applications [1–5]. Despite their ultrathin nature, MSs can impart a nontrivial phase delay on the impinging wave due to the meta-atom resonance, which when spatially modulated is typically exploited for wavefront manipulation [6, 7]. However, this resonant phase delay is inherently dispersive, resulting in narrowband operation. Therefore, conventional metasurfaces can sustain their functionality over very limited bandwidths and fail to perform well for real-world signals which necessarily have significant temporal bandwidth. Thus, researchers have recently focused on the search for broadband (achromatic) MSs that are suitable for practical applications.

Prominent examples of broadband functionalities reported thus far with MSs include wavefront manipulation (e.g., beam steering/splitting, focusing and imaging) [8–12] and pulse delay [13]. Both require a spectrally-constant group delay by the MS [or, equivalently, a linear phase profile $\phi(\omega)$], in order to uniformly delay all frequency components of the broadband input pulse and avoid pulse distortion [Fig. 1(a),(b)]. However, a wider class of very important applications depend on a quadratic phase profile, e.g., dispersion compensation, chirped pulse amplification (CPA), and in general any application requiring control over the instantaneous frequency (chirp) and temporal duration of a broadband input pulse through pulse chirping/dechirping [Fig. 1(c)]. Such operations conventionally require lengthy bulk media, e.g., dispersion compensation fibers in optical telecommunications [Fig. 1(d)].

Thus far, the approaches to dispersion compensation with metasurfaces are scarce [14–17]. They are either very narrowband or do not guarantee pulse integrity. This is because the phase profile is not designed to be purely quadratic across a wide bandwidth (accompanied by a flat amplitude response); rather, typically a single frequency featuring maximum group delay dispersion (GDD) is being exploited [15], Fig. 1(e). In Ref. 16 a broadband pulse is separated into many frequency components and each of them is handled separately by a different, narrowband sub-metasurface. Note that electromagnetically-induced-transparency (EIT) [14] or Huygens' metasurfaces [15] can help to capture the peak of GDD under high transmission. Operation in reflection is not being discussed.

In this work, we present a solution to these problems. We show that by using multiresonant metasurfaces we can overcome the limitations of both traditional, non-resonant approaches (bulky) and modern, singly-resonant metasurfaces (narrowband). Our approach allows to design MSs that implement a general quadratic phase profile which is both arbitrarily strong (despite the ultrathin nature) and (almost) arbitrarily broadband, controlled at will by the number and spacing of the implemented resonances. We derive an explicit construction for the sheet conductivities of a multiresonant surface that can completely control the first three dispersion parameters (phase delay, group delay, and chirp) and discuss the fundamental limitations of physically-possible phase manipulations of broadband chirped pulses by such metasurfaces. We subsequently approximate by finite sequences of physically-realizable Lorentzian resonances

* otsilipakos@eie.gr

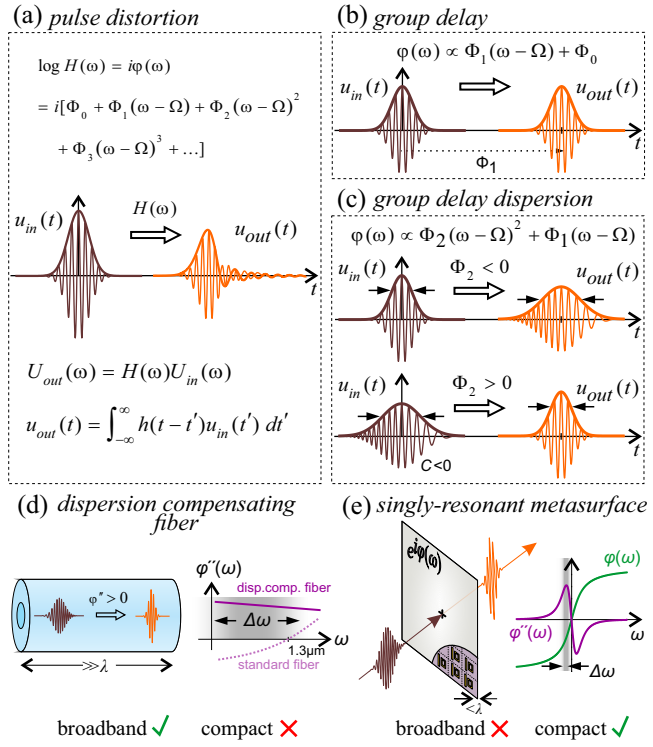

FIG. 1. Motivation and scope of current work. (a) Broadband pulse (centered at frequency Ω) interacting with a medium described by a transfer function of the form $H(\omega) = \exp[i\phi(\omega)]$, where $\phi(\omega) = \Phi_0 + \Phi_1(\omega - \Omega) + \Phi_2(\omega - \Omega)^2 + \ldots$ includes arbitrarily-high orders resulting in pulse distortion. Impact of leading terms of the Taylor expansion on the output pulse shape $u_{\text{out}}(t)$. (b) The first-order term describes pulse delay by $\phi'(\Omega) := d\phi/d\omega|_\Omega = \Phi_1$. The constant Φ_0 leads to a simple shift of the carrier oscillation under the envelope. (c) The second-order term (Φ_2, group delay dispersion) describes pulse chirping (variation of instantaneous frequency along pulse), typically leading to pulse broadening due to the different delay of constituent frequency components (useful for e.g. chirped pulse amplification). For a pre-chirped pulse with chirp parameter C, pulse compression can be achieved when $\Phi_2 C < 0$ (useful for e.g. dispersion compensation). (d,e) Prototypical examples of physical systems for dispersion compensation. (d) Dispersion compensation fiber: The response is broadband but the system is bulky. (e) Conventional singly-resonant metasurface: Thin structure but narrowband operation. Electromagnetically-induced-transparency (EIT) [14] or Huygens metasurfaces [15] can help to capture the peak of group delay dispersion (GDD) under high transmission.

and rigorously quantify the associated error. Both signs of GDD can be implemented and both operation in transmission and reflection mode; as a result, full-space coverage can be provided. Importantly, the required phase delay is solely provided by the resonances implemented on the surface itself. Thus, the proposed surfaces are essentially 2D, apart from a small finite thickness to allow for implementing magnetic polarizability without magnetic materials.

Note that using multiple Lorentzian resonances is the basis of many models meant to capture the response function of solids (susceptibility or permittivity) as accurately as possible. For instance, the Brendel-Borrman model takes into account statistical variations in the vibrational frequencies of amorphous media and models the resulting inhomogeneous broadening by convolving the different Lorentzians with a Gaussian function centered at the respective resonant frequency [18]. Inhomogeneous broadening should have implications for our work as well, since in a realistic metasurface deviations in the meta-atom dimensions along the metasurface would lead to linewidth broadening. In the process of deriving such models, it is important to adhere to the restrictions of causality and the Kramers-Kronig criteria [19]. This means symmetrizing the spectrum of the response function and removing any singularity in the upper complex half-plane [19], which are common elements with our work. Furthermore, ending up with a causal and real-valued time-domain representation of the material response function is also important in the context of time-domain computational electromagnetics (e.g. the Finite-Difference Time Domain Method). In such cases, the efficient incorporation of the material model in the numerical algorithm becomes important as well [20].

II. THEORY OF MULTIRESONANT METASURFACES FOR A QUADRATIC PHASE PROFILE

The main elements of our approach are presented in Fig. 2. Implementing a surface with a very specific multiresonant surface conductivity can provide a perfectly quadratic phase profile $\phi(\omega) = \Phi_2(\omega-\Omega)^2 + \Phi_1(\omega-\Omega) + \Phi_0$ [Fig. 2(a),(b)]. The corresponding slope (GDD) is constant and equals $2\Phi_2$. By making the resonant features denser(sparser) as the frequency increases, a positive(negative) chirp can be implemented; the linewidths of the resonances follow a similar trend. Note that the simpler, special case of equally-spaced resonances would result in a constant (positive) group delay that can be used for delaying broadband pulses [21, 22], see Fig. 2(c). In addition, the linewidth (imaginary part of the complex frequency) is constant for all resonances. A negative constant group delay would require anti-resonances [Fig. 2(d)]. Importantly, operation in transmission and reflection mode can be handled in a uniform manner by spectrally interleaving (antimatching) or overlapping (matching) the electric and magnetic resonances, respectively [Fig. 2(e),(f)].

In order to impart a positive or negative linear chirp (slope of instantaneous frequency) and broaden/compress a broadband Gaussian input pulse, the required response of the metasurface (be it reflection or transmission) should be of the form $H(\omega) = \mathcal{A}\exp\{i[\Phi_2(\omega-\Omega)^2 + \Phi_1(\omega-\Omega) + \Phi_0]\}$, where Ω is the center frequency of the pulse spectrum and $0 < \mathcal{A} \leq 1$

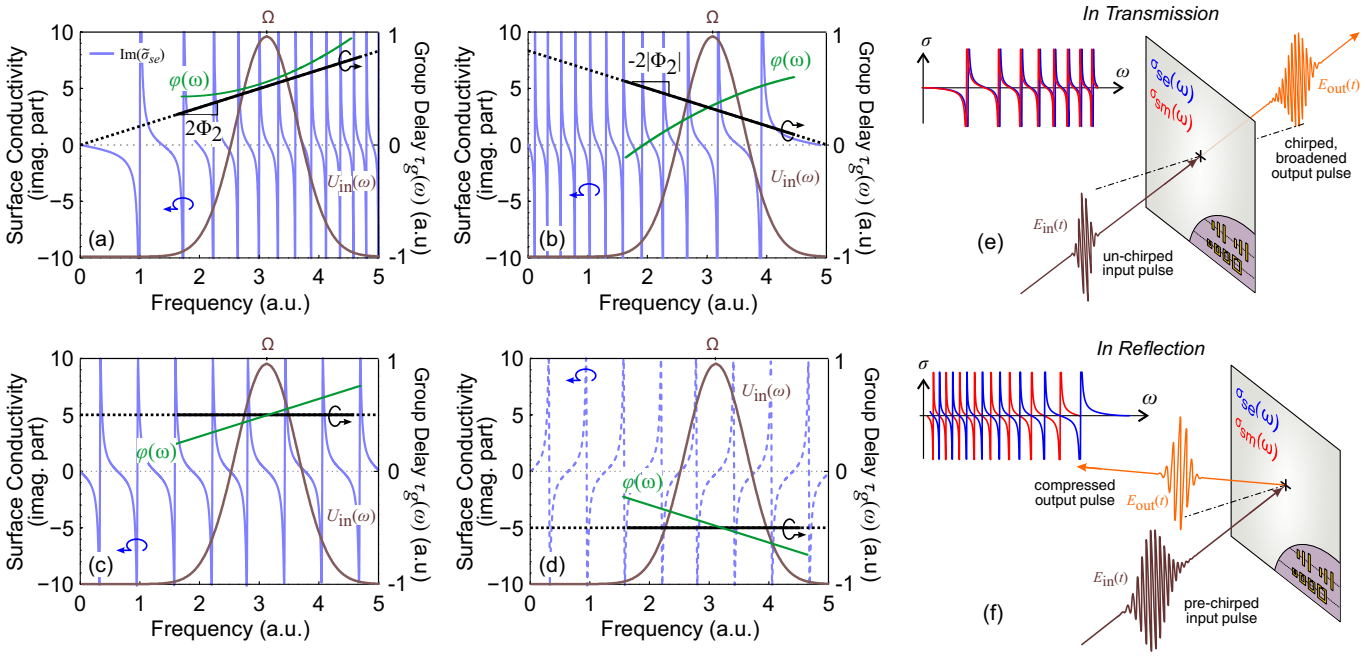

FIG. 2. Proposed multiresonant approach for positive/negative chirp and reflection/transmission operation. Generic multiresonant metasurface with a quadratic transmission/reflection phase profile $[\phi(\omega) = \Phi_2(\omega-\Omega)^2 + \Phi_1(\omega-\Omega) + \Phi_0]$ providing a spectrally-linear group delay of slope GDD $= 2\Phi_2$ for pulse (de-)chirping and pulse broadening/compression. (a) Surface conductivity with multiple resonances of decreasing spacing and linewidth for a positive (constant) slope of the group delay. (b) Multiple resonances of increasing spacing and linewidth for a negative slope. (c) A constant group delay is achieved with equally-spaced resonances [21]. (d) A negative constant group delay would require anti-resonances. (e) An initially un-chirped pulse is temporally broadened and chirped after interacting with the metasurface. Operation in transmission requires overlapping (matched) electric and magnetic resonances. (f) A pre-chirped pulse can be compressed when Φ_2 is of opposite sign. This is the basis of dispersion compensation in e.g. optical fiber systems. Operation in reflection requires interleaved (antimatched) resonances.

allows for some absorption in a realistic MS. With lowercase ϕ_i $(i = 0, 1, 2)$ we indicate coefficients of a Taylor expansion about zero frequency instead of Ω; for relations between capital Φ_i and lowercase ϕ_i see the Supplemental Material (SM) [23], Section S2. Such quadratic transfer functions are used for controlling the group velocity dispersion e.g. in fiber optics [24]. However, $H(\omega)$ is *not* a physical transfer function (TF) since it does not correspond to a real-valued convolution kernel in the time domain, $h(t)$. In order to obey the required Hermitian symmetry, $|X(\omega)| = |X(-\omega)|$ and $\arg X(\omega) = -\arg X(-\omega)$, we introduce the *symmetrized* transfer function $H'(\omega) = \mathcal{A}\exp\{i\,\mathrm{sgn}(\omega)[\Phi_2(|\omega|-\Omega)^2 + \Phi_1(|\omega|-\Omega) + \Phi_0)]\}$, denoted by the prime symbol. Using $H'(\omega)$ in the place of $H(\omega)$ introduces a negligible error as long as the signal half-bandwidth is smaller than the central frequency $(\Delta\omega < \Omega)$, such that the positive-frequency part $g(\omega)$ of the pulse spectrum $U_{\mathrm{in}}(\omega) = g(\omega) + g^*(-\omega)$ of the real input signal does not extend into negative frequencies. For the error to be strictly zero, the support of $g(\omega)$ needs to contain only non-negative frequencies, $g(\omega) = 0\ \forall\ \omega < 0$. For details see SM [23], Section S1.

Although $H'(\omega)$ possesses the correct symmetry, it is discontinuous, i.e., it jumps across the imaginary axis. (In addition, it is not guaranteed to satisfy causality; this will be discussed later on). To side-step this discontinuity, we focus on frequencies $\omega > 0$ for which $H'(\omega)$ is meromorphic; this will allow to use the Mittag-Leffler partial fraction expansion of complex analysis [25]. Note that the analytical continuation of $H'(\omega > 0)$ into negative frequencies coincides with the initially defined $H(\omega)$.

We now specify the required surface conductivities of a MS implementing the transfer function $H'(\omega > 0)$. For operation in transmission, we require scattering amplitudes $t(\omega) = \mathcal{A}e^{i\phi(\omega)}$ and $r(\omega) = 0$, where $\phi(\omega)$ is the quadratic phase. Substituting in the expressions relating plane-wave scattering coefficients with dimensionless conductivities ($\tilde{\sigma}_{se} = \zeta\sigma_{se}/2$ and $\tilde{\sigma}_{sm} = \sigma_{sm}/(2\zeta)$, where ζ is the wave impedance, see SM [23], Section S2), we find (for operation in reflection it would be $\tilde{\sigma}_{sm} = 1/\tilde{\sigma}_{se}$)

$$\tilde{\sigma}_{se} = \tilde{\sigma}_{sm} = -i\tan\left(\frac{\phi(\omega) + i|\log\mathcal{A}|}{2}\right) = -i\tan z(\omega). \quad (1)$$

Equation 1 constitutes the "target spectrum" of the conductivities. However, only certain types of resonant behavior are available in nature. In the following, we will thus be seeking a good approximation of the target spectrum using Lorentzian resonances, which can be physically implemented with resonant meta-atoms. The $\omega-$poles for the desired conductivities of Eq. (1) can

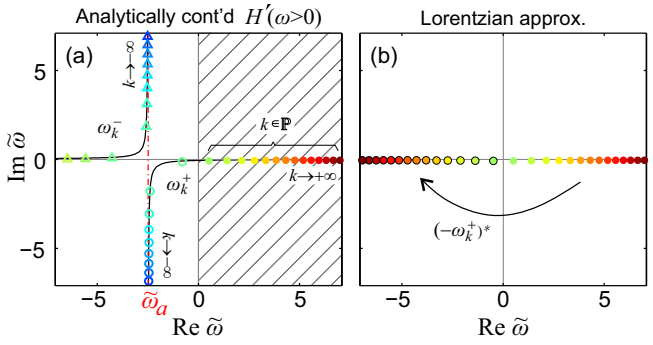

FIG. 3. (a) Positions of poles of Eq. (1) in the complex $\omega-$plane assuming the analytically-continued transfer function $H'(\omega>0)$. The two branches, ω_k^+ and ω_k^-, diverge at $\mathrm{Re}(\omega)=\omega_a$. A subset of the poles of the ω_k^+ branch satisfies $\mathrm{Re}\,\omega_k^+>0$ and $\mathrm{Im}\,\omega_k^+<0$ and is denoted by $k\in\mathbb{P}$. (b) Strategy for Lorentzian approximation: the $k\in\mathbb{P}$ poles in panel (a) are used along with their negative-conjugate counterparts. This specific example is for $\phi_2=+0.25$, $\phi_1=2.48$, $\phi_0=0$, and $\mathcal{A}=0.7$. The normalized frequency is defined as $\tilde{\omega}=\omega\sqrt{|\Phi_2|}$ and the normalized apex frequency equals $\tilde{\omega}_a=-2.48$. Note that all the poles in panel (b) satisfy $\mathrm{Im}\,\omega<0$; the imaginary part is small and they might seem to overlap with the horizontal axis. For the particular poles depicted in panel (b) it holds $-0.0585<\mathrm{Im}\,\tilde{\omega}<-0.0187$.

be found analytically by solving a quadratic equation (SM [23], Section S2), resulting in two sets of poles in the complex ω-plane

$$\omega_k^{\pm}=:\omega_a\pm\omega_k=\Omega-\frac{\Phi_1}{2\Phi_2}\pm\sqrt{\left(\frac{\Phi_1}{2\Phi_2}\right)^2+\frac{1}{\Phi_2}\left[(2k+1)\pi-\Phi_0-i|\log\mathcal{A}|\right]},\tag{2}$$

where ω_a is a real quantity coinciding with the apex of the parabolic phase and ω_k a complex quantity that determines the offset of the poles in the complex plane. The poles reside on two curves which asymptotically approach the vertical axis $\mathrm{Re}(\omega)=\omega_a$ for $k\to-\infty$ and the horizontal axis $\mathrm{Im}(\omega)=0$ for $k\to+\infty$. Depending on the specific choice for Φ_i, the index k is "re-normalized" and the poles shift to different discrete positions along the curves (see SM [23], Section S2). The discrete poles along with the underlying continuous curves are depicted in Fig. 3(a) for a characteristic positive-chirp ($\Phi_2>0$) case. Note that the pole index k is under the square root, leading to non-uniform spacing along the real axis and a varying imaginary part, in contrast to the case of multiresonant metasurfaces for pulse delay [21], where the poles are equidistant and the imaginary part constant. The study of pole structure in nanophotonics and metasurfaces/scatterers in particular is recently receiving increased interest, since it can help to achieve advanced functionalities and provide physical insight [26–33].

In Fig. 3(a) we have chosen $\Phi_1>2\Phi_2\Omega$ so that ω_a, where the two branches diverge, lies in the left complex half-plane. When $\omega_a<0$, *all* the poles in the right complex half-plane are predominantly real *and* possess a negative imaginary part. They are compatible with physical resonances and can form the basis for a Lorentzian approximation discussed below [see Fig. 3(b)]; poles to the left of ω_a possess a positive imaginary part and would not satisfy causality (anti-resonances). Importantly, this means that there is no fundamental limit on the bandwidth that can be accommodated by the metasurface; in contrast, if $\omega_a>0$ a low-frequency limit for the positive-frequency content of the pulse would be imposed.

Having specified the simple $\omega-$poles of Eq. (1), we can write the corresponding Mittag-Leffler expansion (see SM [23], Section S3)

$$-i\tan z(\omega)=\sum_{k=-\infty}^{+\infty}\frac{i}{\omega_k\Phi_2}\left(\frac{1}{\omega-\omega_k^+}-\frac{1}{\omega-\omega_k^-}\right).\tag{3}$$

The residues are $r_k^+=i/(\omega_k\Phi_2)$ and $r_k^-=-i/(\omega_k\Phi_2)$ for ω_k^+ and ω_k^- poles, respectively. We now identify a subset of the poles of the ω_k^+ branch that satisfies $\mathrm{Re}\,\omega_k^+>0$ and $\mathrm{Im}\,\omega_k^+<0$ and can play the role of positive-frequency poles of an underdamped linear oscillator (resonant meta-atom), see SM [23] (Section S3.A). The corresponding indices are denoted by $k\in\mathbb{P}$ in Fig. 3(a). We can thus use these simple poles, along with their complex conjugate counterparts, to construct a physical, Lorentzian approximation of the target spectrum. This procedure is schematically depicted in Fig. 3(b). Looking at the form of a Lorentzian resonance in the surface conductivity (see SM [23], Section S3.A), we also require that the corresponding residues are of the form $r_k^+=a(i\omega_k^+)$, with $a\in\mathbb{R}$ and $a>0$. This suggests approximating the actual residues with $r_k^+=i/(\omega_k\Phi_2)\approx\mathrm{Re}[1/(\omega_k\Phi_2\omega_k^+)]i\omega_k^+$. For any reasonable value of loss, the $k\in\mathbb{P}$ poles are predominantly real and the error of approximating the residues by taking the real part is negligible. The Lorentzian approximation (LA) then takes the form

$$\tilde{\sigma}_{\mathrm{LA}}(\omega)=\sum_{k\in\mathbb{P}}\mathrm{Re}\left(\frac{1}{\omega_k\Phi_2\omega_k^+}\right)\left(\frac{i\omega_k^+}{\omega-\omega_k^+}-\frac{(i\omega_k^+)^*}{\omega-(-\omega_k^+)^*}\right).\tag{4}$$

Note that by construction the proposed response function given by Eq. (4) is analytic in the upper half-plane and of Hermitian symmetry (the time-domain counterpart is real). In addition, for a finite number of terms it also holds $\tilde{\sigma}_{\mathrm{LA}}(\omega)\to0$ as $|\omega|\to\infty$. This means that the real and imaginary parts are related via Kramers-Kronig relations (see e.g. Ref.34. What remains in $\tilde{\sigma}(\omega)=-i\tan z(\omega)=\tilde{\sigma}_{\mathrm{LA}}(\omega)+\Delta\tilde{\sigma}(\omega)$ is the error of the Lorentzian approximation and is comprised of four contributions: (i) the subtraction of the negative frequency counterparts we added in Eq. (4), (ii) what is left from taking the real part of the residues, (iii) the poles omitted from the ω_k^+ branch ($k\notin\mathbb{P}$), and (iv) the entire ω_k^- branch. See SM [23] (Section S3.B) for details.

The procedure is entirely analogous for a negative chirp ($\Phi_2 < 0$). In this case, necessarily $\omega_a > 0$ and only poles in the strip $\mathrm{Re}(\omega) \in (0, \omega_a)$ can be used for the LA; this imposes a high-frequency limit for the positive-frequency content of the pulse [see SM [23], Fig. S2(b)].

It is also interesting to note that not only the proposed response function, $\tilde{\sigma}_{\mathrm{LA}}(\omega)$, but also the corresponding transfer function $t = (1 - \tilde{\sigma}_{\mathrm{LA}})/(1 + \tilde{\sigma}_{\mathrm{LA}})$ (we have used $\tilde{\sigma}_{se}(\omega) = \tilde{\sigma}_{sm}(\omega) = \tilde{\sigma}_{\mathrm{LA}}(\omega)$ in Eq. (S18b) of the SM) is analytic in the upper half-plane. This is discussed in more detail in SM [23], Section S4. The corresponding scattered field, $t(\omega) - 1$ (the total transmitted field is the sum of incident field plus scattered field), possesses the additional property that it vanishes at infinity (for a finite sum of Lorentzians). We thus conclude that Kramers-Kronig relations apply to the scattered field, $t(\omega) - 1$.

III. TRUNCATION OF INFINITE LORENTZIAN SUM AND PERFORMANCE ANALYSIS

The final step that enables a practical, physical prescription for the implementation of a metasurface for dispersion compensation and pulse chirping is to truncate the sum in Eq. (4). The impact of this truncation on the MS performance is tractable and the associated error is negligible provided that the pulse spectrum is accommodated within the bandwidth supplied by the finite set of resonances. This is demonstrated in Fig. 4 and 5, where the effect of the LA and its truncation on the transfer function of the MS, as well as the pulse in the time domain, are documented.

Figure 4 deals with positive chirp ($\Phi_2 > 0$) and studies compression (dispersion compensation) of a negatively pre-chirped ($C < 0$) broadband Gaussian pulse upon interaction with the metasurface. The input pulse is a delayed, modulated Gaussian pulse of the form $u_{\mathrm{in}}(t) = \exp[-(1+iC)(t-t_0)^2/(2\tau_0^2)]\exp[-i\Omega(t-t_0)]$, with $\Delta\omega = 1/\tau_0$ being the transform limited spectral half-width (e^{-1} intensity point) of the pulse spectrum. The parameters of the example are: $\Omega = 2\pi \times 4.5 \cdot 10^9$ rad/s, initial chirp $C = -1$, $\Delta\omega = 1/\tau_0 = 2\pi \times 0.28 \cdot 10^9$ rad/s, $\mathcal{A} = 0.95$, $\Phi_2 = +0.04$ ps^2, $\Phi_1 = 2.26$ ps, $\Phi_0 = 32$ (equivalently, $\phi_2 = 0.04$ ps^2, $\phi_1 = 0$, $\phi_0 = 0$). Microwave frequencies are selected for this example, since for the physical implementation we can directly rely on an experimentally-verified multiresonant unit cell based on ELC (electric-LC) electric resonators and SRR (split ring resonator) magnetic resonators [13]. The approach of using metallic meta-atoms can be utilized practically unchanged up to THz frequencies. For optical frequencies, Mie resonances in dielectric particles may constitute a favorable approach, since metals are associated with significant resistive loss. Note that such engineering challenges, associated with a particular physical implementation, are outside the scope of the current work, in which we establish the theoretical principles and foundations that

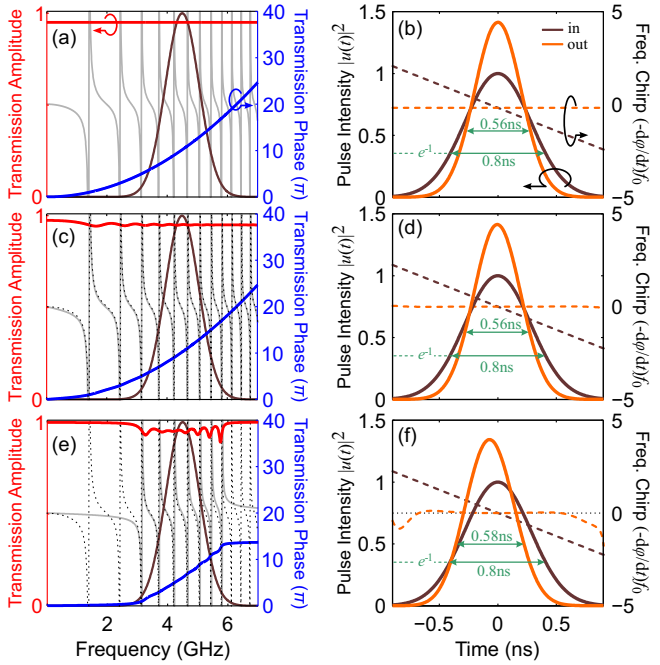

FIG. 4. Results for operation in transmission. Compression of a negatively pre-chirped ($C < 0$) Gaussian broadband pulse upon interaction with a metasurface exhibiting a quadratic phase profile with positive Φ_2 (e.g. for dispersion compensation). Different levels of approximation in the transfer function and impact on the output pulse $u_{\mathrm{out}}(t)$. (a,b) Ideal transfer function: (a) Ideal transmission amplitude and phase; some loss is included ($\mathcal{A} := |t(\omega)| = 0.95$). The corresponding required surface conductivity and the pulse spectrum are overlaid. (b) Input and output pulse and frequency chirp. The output pulse is de-chirped and compressed by $1/\sqrt{2}$, as verified by the pulse durations measured at the e^{-1} intensity points. (c,d) Physical approximation of the ideal target spectrum with an infinite train of Lorentzian resonances [Eq. (4)]: (c) Transmission amplitude and phase along with surface conductivity and pulse spectrum. The ideal surface conductivity from panel (a) is also included with a dashed line. (d) Input and output pulse and frequency chirp. The performance is practically indistinguishable from the ideal case. (e,f) Truncated physical approximation using seven resonances: (e) Some ripples manifest in the transmission phase/amplitude due to the truncation. The untruncated surface conductivity from panel (c) is included with a dashed line. (f) The compression is only slightly affected and the residual output chirp is negligible along the duration of the output pulse.

are prerequisite to any subsequent physical implementation. The target spectrum is depicted in Fig. 4(a): the transmission amplitude is flat and equal to 0.95 over arbitrarily-broad bandwidths and the phase is exactly quadratic. In effect, the input pulse is compressed by exactly $1/\sqrt{2}$, as designed, and the output chirp (variation of instantaneous frequency) is zero across the entire pulse duration [Fig. 4(b)]. The untruncated train of physical Lorentzian resonances [Eq. (4)] is depicted in Fig. 4(c). The target spectrum is included with a dashed line; they

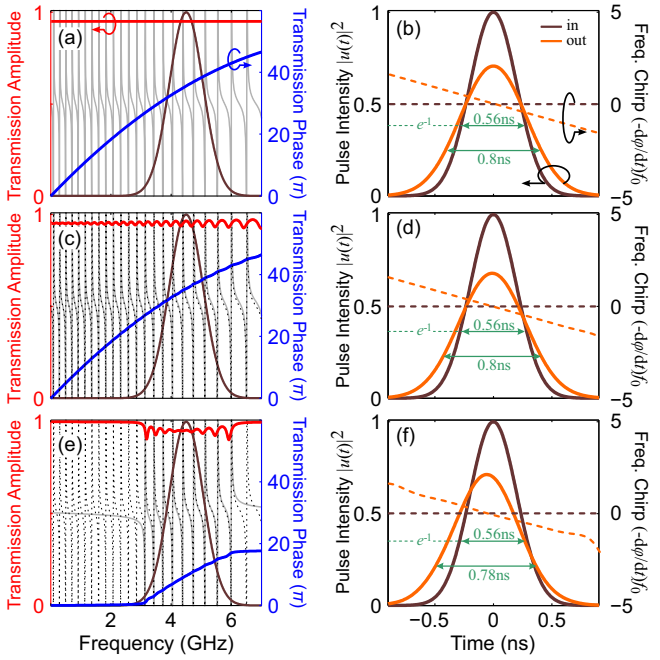

FIG. 5. Results for operation in transmission. Broadening of an initially un-chirped Gaussian broadband pulse upon interaction with a metasurface exhibiting a quadratic phase profile with negative Φ_2 (e.g. for chirped pulse amplification). Different levels of approximation in the transfer function and impact on the output pulse $u_{\rm out}(t)$. (a,b) Ideal transfer function: (a) Ideal transmission amplitude and phase; some loss is included ($\mathcal{A} := |t(\omega)| = 0.95$). The corresponding required surface conductivity and the pulse spectrum are overlaid. (b) Input and output pulse and frequency chirp. The output pulse acquires a negative chirp and is broadened by $\sqrt{2}$, as verified by the pulse durations measured at the e^{-1} intensity points. (c,d) Physical approximation of the ideal target spectrum with an infinite train of Lorentzian resonances: (c) Transmission amplitude and phase along with surface conductivity and pulse spectrum. The ideal surface conductivity from panel (a) is also included with a dashed line. (d) Input and output pulse and frequency chirp. The performance is practically indistinguishable from the ideal case. (e,f) Truncated physical approximation with nine resonances: (e) The untruncated surface conductivity from panel (c) is also included with a dashed line. (f) The broadening is only slightly affected; the output chirp is in good approximation linear along the duration of the output pulse.

are almost indistinguishable and so is the effect on the output pulse [Fig. 4(d)]. Subsequently, the infinite resonance train is truncated keeping only seven resonances [Fig. 4(e)]. The available bandwidth becomes finite but is approximately 3 GHz, corresponding to a vast relative bandwidth of 67%. Due to the crude truncation, a ripple develops in the transmission amplitude and phase. However, the pulse compression is only slightly affected and the residual output chirp is negligible throughout the duration of the output pulse [Fig. 4(f)]. If even higher integrity is required, one can fine-tune the positions and strengths of the considered resonances after truncation and/or introduce an additional background contribution [see SM [23], Fig. S5(d)].

Next, the case of negative chirp ($\Phi_2 < 0$) and pulse stretching (e.g. for chirped pulse amplification) is considered in Fig. 5. The parameters of the example are: $\Omega = 2\pi \times 4.5 \cdot 10^9$ rad/s, initial chirp $C = 0$, $\Delta\omega = 2\pi \times 0.28 \cdot 10^9$ rad/s (transform-limited spectral half-width, e^{-1} intensity point), $\mathcal{A} = 0.95$, $\Phi_2 = -0.04$ ps^2, $\Phi_1 = 2.83$ ps, $\Phi_0 = 112$ (equivalently, $\phi_2 = -0.04$ ps^2, $\phi_1 = 5.1$ ps, $\phi_0 = 0$). The target spectrum is depicted in Fig. 5(a). The initially un-chirped Gaussian broadband pulse acquires a linear induced chirp and is broadened by a factor $\sqrt{2}$, as designed [Fig. 5(b)]. The infinite Lorentzian approximation is depicted in Fig. 5(c). As was the case with the positive chirp scenario, the output pulse [Fig. 5(d)] is almost indistinguishable compared with the ideal case. Finally, the infinite resonance train is truncated keeping nine resonances [Fig. 5(e)]. Pulse stretching is only slightly affected and output chirp is linear throughout the duration of the output pulse [Fig. 5(f)]. Results for operation in reflection mode (both positive and negative chirp) are included in the SM [23], Section S5.

IV. CONCLUSION

In conclusion, we have presented a solution to arbitrarily-strong and arbitrarily-broadband quadratic phase shaping with multiresonant metasurfaces. Our approach aspires to bring dispersion engineering to the nanoscale and overcome the current limitations of both (i) conventional, non-resonant approaches with bulk media (too bulky) as well as (ii) modern, singly-resonant metasurfaces (too narrowband). The proposed concept is not limited to dispersion compensation or chirped pulse amplification, but provides a generic and powerful ultrathin platform for the spatio-temporal control of broadband real-world signals with a myriad of applications in modern optics, microwave photonics, radar and communication systems.

ACKNOWLEDGMENTS

Work at Ames Laboratory was supported by the Department of Energy (Basic Energy Sciences, Division of Materials Sciences and Engineering) under Contract No. DE-AC02-07CH11358. Support by the Hellenic Foundation for Research and Innovation (H.F.R.I.) under the "2nd Call for H.F.R.I. Research Projects to support Postdoctoral Researchers" (Project Number: 916, PHOTOSURF).

[1] S. B. Glybovski, S. A. Tretyakov, P. A. Belov, Y. S. Kivshar, and C. R. Simovski, Metasurfaces: From microwaves to visible, Phys. Rep. **634**, 1 (2016).

[2] H.-T. Chen, A. J. Taylor, and N. Yu, A review of metasurfaces: Physics and applications, Rep. Prog. Phys. **79**, 076401 (2016).

[3] Q. He, S. Sun, and L. Zhou, Tunable/reconfigurable metasurfaces: Physics and applications, Research **2019**, 1849272 (2019).

[4] S. Sun, Q. He, J. Hao, S. Xiao, and L. Zhou, Electromagnetic metasurfaces: physics and applications, Adv. Opt. Photonics **11**, 380 (2019).

[5] O. Tsilipakos, A. C. Tasolamprou, A. Pitilakis, F. Liu, X. Wang, M. S. Mirmoosa, D. C. Tzarouchis, S. Abadal, H. Taghvaee, C. Liaskos, A. Tsioliaridou, J. Georgiou, A. Cabellos-Aparicio, E. Alarcón, S. Ioannidis, A. Pitsillides, I. F. Akyildiz, N. V. Kantartzis, E. N. Economou, C. M. Soukoulis, M. Kafesaki, and S. Tretyakov, Toward intelligent metasurfaces: The progress from globally tunable metasurfaces to software-defined metasurfaces with an embedded network of controllers, Advanced Optical Materials **8**, 2000783 (2020).

[6] N. M. Estakhri, V. Neder, M. W. Knight, A. Polman, and A. Alù, Visible light, wide-angle graded metasurface for back reflection, ACS Photonics **4**, 228 (2017).

[7] V. S. Asadchy, A. Wickberg, A. Díaz-Rubio, and M. Wegener, Eliminating scattering loss in anomalously reflecting optical metasurfaces, ACS Photonics **4**, 1264 (2017).

[8] S. Wang, P. C. Wu, V.-C. Su, Y.-C. Lai, C. Hung Chu, J.-W. Chen, S.-H. Lu, J. Chen, B. Xu, C.-H. Kuan, T. Li, S. Zhu, and D. P. Tsai, Broadband achromatic optical metasurface devices, Nat. Commun. **8**, 187 (2017).

[9] W. T. Chen, A. Y. Zhu, V. Sanjeev, M. Khorasaninejad, Z. Shi, E. Lee, and F. Capasso, A broadband achromatic metalens for focusing and imaging in the visible, Nat. Nanotechnol. **13**, 220 (2018).

[10] S. Shrestha, A. C. Overvig, M. Lu, A. Stein, and N. Yu, Broadband achromatic dielectric metalenses, Light Sci. Appl. **7**, 85 (2018).

[11] A. A. Fathnan, M. Liu, and D. A. Powell, Achromatic Huygens' metalenses with deeply subwavelength thickness, Advanced Optical Materials **8**, 2000754 (2020).

[12] O. Tsilipakos, M. Kafesaki, E. N. Economou, C. M. Soukoulis, and T. Koschny, Squeezing a prism into a surface: Emulating bulk optics with achromatic metasurfaces, Advanced Optical Materials **8**, 2000942 (2020).

[13] O. Tsilipakos, L. Zhang, M. Kafesaki, C. M. Soukoulis, and T. Koschny, Experimental implementation of achromatic multiresonant metasurface for broadband pulse delay, ACS Photonics **8**, 1649 (2021).

[14] B. Dastmalchi, P. Tassin, T. Koschny, and C. M. Soukoulis, Strong group-velocity dispersion compensation with phase-engineered sheet metamaterials, Phys. Rev. B **89**, 10.1103/physrevb.89.115123 (2014).

[15] M. Decker, I. Staude, M. Falkner, J. Dominguez, D. N. Neshev, I. Brener, T. Pertsch, and Y. S. Kivshar, High-efficiency dielectric Huygens' surfaces, Adv. Opt. Mater. **3**, 813 (2015).

[16] S. Divitt, W. Zhu, C. Zhang, H. J. Lezec, and A. Agrawal, Ultrafast optical pulse shaping using dielectric metasurfaces, Science **364**, 890 (2019).

[17] E. Rahimi and K. Şendur, Femtosecond pulse shaping by ultrathin plasmonic metasurfaces, J. Opt. Soc. Am. B **33**, A1 (2016).

[18] R. Brendel and D. Bormann, An infrared dielectric function model for amorphous solids, Journal of Applied Physics **71**, 1 (1992).

[19] J. Orosco and C. F. M. Coimbra, Optical response of thin amorphous films to infrared radiation, Phys. Rev. B **97**, 094301 (2018).

[20] L. J. Prokopeva, S. Peana, and A. V. Kildishev, Gaussian dispersion analysis in the time domain: Efficient conversion with padé approximants, Computer Physics Communications **279**, 108413 (2022).

[21] O. Tsilipakos, T. Koschny, and C. M. Soukoulis, Antimatched electromagnetic metasurfaces for broadband arbitrary phase manipulation in reflection, ACS Photon. **5**, 1101 (2018).

[22] V. Ginis, P. Tassin, T. Koschny, and C. M. Soukoulis, Broadband metasurfaces enabling arbitrarily large delay-bandwidth products, Appl. Phys. Lett. **108**, 031601 (2016).

[23] See Supplemental Material at `url` for for (i) a thorough discussion of the fundamental physical constraints in deriving a proper metasurface transfer function for pulse chirping, (ii) the analytic structure of sheet conductivities that implement the transfer function, (iii) the rigorous derivation of the partial fraction expansion and multi-resonant Lorentzian approximation as well as the assessment of the associated error before and after truncation, (iv) the analyticity of the transfer function (transmission/reflection) and (v) complementary results for operation in reflection.

[24] G. P. Agrawal, *Nonlinear Fiber Optics*, 4th ed. (Academic Press, 2006).

[25] M. J. Ablowitz and A. S. Fokas, *Complex Variables, Introduction and Applications*, 2nd ed. (Cambridge University Press, 2003).

[26] M. Benzaouia, J. D. Joannopoulos, S. G. Johnson, and A. Karalis, Analytical criteria for designing multiresonance filters in scattering systems, with application to microwave metasurfaces, Physical Review Applied **17**, 10.1103/physrevapplied.17.034018 (2022).

[27] R. Colom, E. Mikheeva, K. Achouri, J. Zuniga-Perez, N. Bonod, O. J. F. Martin, S. Burger, and P. Genevet, Crossing of the branch cut: The topological origin of a universal 2π-phase retardation in non-hermitian metasurfaces, Laser & Photonics Reviews **2023**, 2200976 (2023).

[28] T. Wu, A. Baron, P. Lalanne, and K. Vynck, Intrinsic multipolar contents of nanoresonators for tailored scattering, Physical Review A **101**, 10.1103/physreva.101.011803 (2020).

[29] A. Gras, W. Yan, and P. Lalanne, Quasinormal-mode analysis of grating spectra at fixed incidence angles, Optics Letters **44**, 3494 (2019).

[30] V. Grigoriev, A. Tahri, S. Varault, B. Rolly, B. Stout, J. Wenger, and N. Bonod, Optimization of resonant effects in nanostructures via weierstrass factorization, Physical Review A **88**, 10.1103/physreva.88.011803 (2013).

[31] C. Valagiannopoulos, Stable electromagnetic interactions with effective media of active multilayers, Phys. Rev. B **105**, 045304 (2022).
[32] A. F. Tzortzakakis, K. G. Makris, A. Szameit, and E. N. Economou, Transport and spectral features in non-hermitian open systems, Phys. Rev. Research **3**, 013208 (2021).
[33] T. Christopoulos, E. E. Kriezis, and O. Tsilipakos, Multimode non-hermitian framework for third harmonic generation in nonlinear photonic systems comprising two-dimensional materials, Phys. Rev. B **107**, 035413 (2023).
[34] J. Bechhoefer, Kramers–Kronig, Bode, and the meaning of zero, American Journal of Physics **79**, 1053 (2011).